Ultra-Sharp Transmission Resonances in Periodic Arrays of Graphene Ribbons in TE Polarization

Amin Khavasi

***Abstract*—When illuminated by TM polarized waves, periodic arrays of graphene ribbons are known to exhibit plasmonic resonances due to their dual inductive–capacitive nature. It is demonstrated here that even in TE polarization, resonances can be observed in these structure. These resonances, which are of nonplasmonic origin, are explained by means of a circuit model. It is shown that, for a certain frequency range, arrays of graphene ribbons have both capacitive and inductive properties, which lead to an ultra-sharp inductor–capacitor resonance. The banwidth of this resonance can be as narrow as ∼0.0002 nm at a wavelength of 630 nm. The resonance can also be viewed as the grating excitation of a TE mode on graphene. The resonance properties in terms of different parameters are also invedtigated.**

***Index Terms*—Circuit theory, graphene, sharp resonance.**

I. Introduction

GRAPHENE has attracted great attention in recent years due to its stability and exceptional optoelectronic properties [1]–[3]. Several applications such as high-speed transistors [4], broadband optical modulators [5], ultrafast photodetectors [6] and transparent conducting electrodes [7] have already been demonstrated by using graphene. It has also been demonstrated that periodically patterned graphene supports relatively broadband TM resonances [8]–[10], which can be utilized in different applications such as broadband absorbers [11] and metasurface conformal cloaks [12]. These resonances are due to dual inductive–capacitive nature of the structure [13], [14] which stems from the excitation of localized plasmon modes [15] on the graphene patches.

In this paper, periodic arrays of graphene ribbons (PAGRs) are studied in TE polarization where the electric field vector is parallel to the ribbons. In particular, we focus on the frequency range in which the imaginary part of the surface conductivity of graphene is positive. The graphene ribbons can then be considered as ultra-thin dielectric patches. Since dielectric gratings are known to support guided-mode resonances [17], similar effect is expected in PAGRs.

To describe this effect, we propose a simple and accurate circuit model for PAGRs in TE polarization which resembles the model for a periodic array of nanowires with finite conductivity [16]. It is demonstrated that, in the frequency range where the surface conductivity of graphene has a positive imaginary part, the PAGR has dual capacitive-inductive nature, and can exhibit *LC* resonances. In contrast to TM resonance which is relatively broadband and is observed in the sub-wavelength regime, the TE resonance is ultra-sharp and occurs just before the onset of the first diffracted order. Moreover, whereas the TM resonance is of plasmonic nature [14], the TE resonance takes place when graphene can be considered as an ultrathin dielectric.

The paper is organized as follows: In Section II, we propose a circuit model for PAGRs in TE polarization and we explain the possibility of observing a resonance according to the circuit model. In Section III, the simulation results are presented and the existence of the resonance is demonstrated. We also describe the link between this phenomenon and the well-known guided mode resonance already studied in dielectric gratings. Moreover, the behavior of resonance versus graphene width to period ratio, and number of graphene layers is investigated in this section. Finally, conclusions are drawn in Section IV.

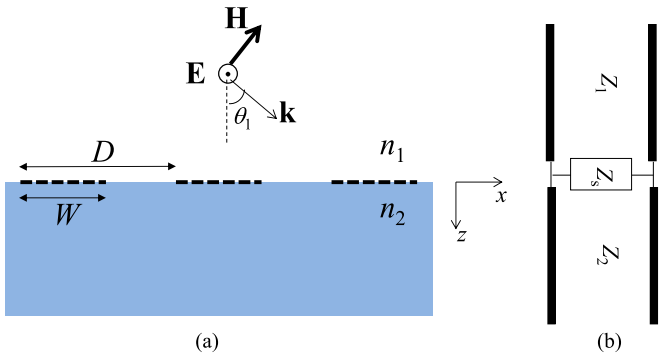

Fig. 1. (a) The structure under study: A PAGR surrounded by two media with refractive indices of n_1 and n_2. (b) The proposed circuit model for the structure.

II. Circuit Model for PAGRs in TE Polarization

Consider a PAGRs with period *D*, as shown in Fig. 1(a). Graphene ribbons, depicted by dashed lines, are infinitely long in the *y*-direction and have a width of *W*. The structure is illuminated from the upper medium by a TE polarized plane wave with a vacuum wavelength λ. The angle of incidence is θ_1. The refractive indices of the upper and lower media are n_1 and n_2, respectively. The graphene ribbons are modeled using a surface conductivity σ_s, which can be derived from the well-known Kubo formula [17] and is given by:

$$\sigma_s = \frac{2e^2 k_B T}{\pi\hbar^2}\frac{j}{j\tau^{-1}-\omega}\ln\left[2\cosh\left(\frac{E_F}{2k_BT}\right)\right] + \frac{je^2}{4\pi\hbar}\ln\left[\frac{2E_F+\hbar(\omega-j\tau^{-1})}{2E_F-\hbar(\omega-j\tau^{-1})}\right] \quad (1)$$

Manuscript received February 21, 2015; revised May 30, 2015, June 28, 2015, July 31, 2015, and August 9, 2015; accepted August 9, 2015. Date of publication November 23, 2015; date of current version February 5, 2016.

The author is with the Electrical Engineering Department, Sharif University of Technology, Tehran 11155-4363, Iran (e-mail: khavasi@sharif.edu).

Color versions of one or more of the figures in this paper are available online at http://ieeexplore.ieee.org.

Digital Object Identifier 10.1109/JLT.2015.2502064

where e is the electron charge, k_B is the Boltzmann constant, $\hbar$ is the Plank constant, T is the temperature, E_F is the Fermi energy, ω is the angular frequency and τ is the relaxation time. We set $T = 300$ K, $E_F = 1$ eV and $\tau = 1$ ps throughout this work. A time-dependence of $e^{j\omega t}$ is assumed and suppressed throughout this paper.

The proposed circuit model is illustrated in Fig. 1(b), where the surrounding homogenous regions are modeled as transmission lines with the characteristic impedances

$$Z_i = \eta_0/(n_i \cos\theta_i), \quad i = 1, 2 \tag{2}$$

where $\eta_0 \cong 120\,\pi$ is the free space impedance, and θ_2 is the angle of refracted wave in the lower medium.

The PAGR is represented by a shunt impedance of Z_s,

$$Z_s = j\omega \frac{L_1 L_2}{L_1 + L_2} + Z_G \tag{3}$$

where L_1 and L_2 are the equivalent inductances of a periodic array of perfectly conducting sheets and represent the magnetic energy stored in the upper and lower media, respectively. The two inductors are in parallel with each other and their values are given by the following expression [18]:

$$L_i = \frac{\eta_0 D}{c_0 \pi} \ln\left[\csc\left(\frac{\pi W}{2D}\right)\right] \left(1 - \alpha + \frac{\alpha}{\sqrt{1 - (\lambda_{ci}/\lambda)^2}}\right), \quad i = 1, 2 \tag{4}$$

where c_0 is the free space speed of light, $\lambda_{ci} = n_i(1 + \sin(\theta_i))D$ and $\alpha \approx \sqrt{1 - [(D - W)/D]^4}$. In (3), Z_G is the impedance due to the finite conductivity of graphene. For evaluating Z_G, let us follow the approach of [16]: writing the Ampere's law over one period of the PAGR, calculating the ratio of the dissipated power in graphene, and equating it with that in Z_G. The sought-after impedance Z_G, is then obtained as:

$$Z_G = \frac{D}{\sigma_s W}. \tag{5}$$

At low frequencies, $\hbar\omega < 1.667\,E_F$ [19], the first term in (1), the intraband contribution, is dominant and thus the imaginary part of the surface conductivity is negative (see Fig. 2). Therefore, the imaginary part of Z_G is positive and from (3) the impedance of PAGR is inductive and no resonance is expected. However, at higher frequencies the second term, the interband contribution, is not negligible. This term dominates for $\hbar\omega > 1.667\,E_F$ and thus the imaginary part of the surface conductivity becomes positive as it is seen in Fig. 2. This implies that Z_G is capacitive and a *LC* resonance can be observed. It can be easily shown that if $\lambda \ll \lambda_{ci}$ the impedance of L_1 and L_2 will be far smaller than Z_G. However, according to (4) the inductances L_1 and L_2 tend to extremely large values at wavelengths slightly larger than λ_{ci}. Thus the *LC* resonance is expected to occur just before the onset of the first diffracted order. It should be also noted that inasmuch as L_1 and L_2 are parallel, both must have large inductances in order to achieve large equivalent inductance. This requires that $\lambda_{c1} \approx \lambda_{c2}$ or equivalently $n_1 \approx n_2$.

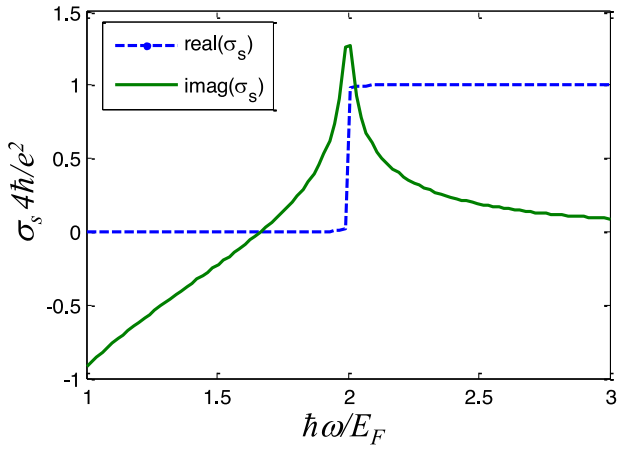

Fig. 2. Real and imaginary part of graphene surface conductivity.

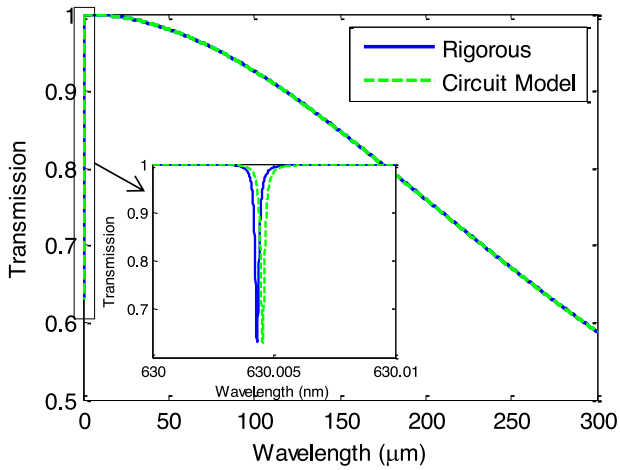

Fig. 3. Transmission of the structure shown in Fig. 1 at normal incidence and with $D = 630$ nm, $W = 0.2\,D$, $n_1 = n_2 = 1$. The inset shows the ultra-sharp *LC* resonance. A monolayer graphene is used in this simulation.

III. Results and Discussion

Based on the argument given in the previous section, the following parameters were chosen, $D = 630$ nm, $W = 0.2\,D$, $n_1 = n_2 = 1$ and $\theta_1 = 0$, to ensure observation of a resonance near $\lambda_{ci} = D$. The transmission of this structure, calculated by the proposed circuit model, is illustrated in Fig. 3 which is in excellent agreement with the rigorous results obtained by Fourier modal method (FMM) [20]. An ultra-sharp resonance is also observed at $\lambda = 630.004$ nm with a bandwidth of $\Delta\lambda$ 0.00017 nm. Nonetheless, it may be difficult to excite such a narrowband resonance experimentally. Therefore, as the second example, a PAGR consisting of five graphene layers is studied. The other parameters are the same as the previous example. The surface current on a five-layer graphene is five times of that on a monolayer graphene. Therefore, to model this configuration, the surface conductivity is multiplied by 5. The transmission is plotted in Fig. 4, and the resonance, observed at $\lambda = 630.109$ nm, has a bandwidth of $\Delta\lambda \sim 0.0081$ nm. The surface current density on graphene at resonance wavelength is also illustrated in Fig. 5. It is similar to a part of a sinusoidal

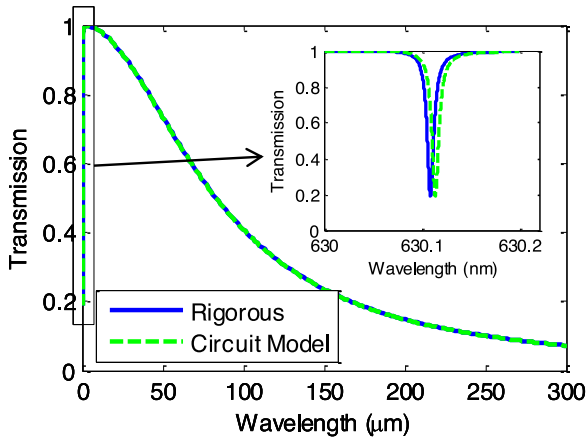

Fig. 4. Transmission of the structure shown in Fig. 1 at normal incidence and with $D = 630$ nm, $W = 0.2\ D$, $n_1 = n_2 = 1$. The inset shows the ultra-sharp *LC* resonance. A five-layer graphene is used in this simulation.

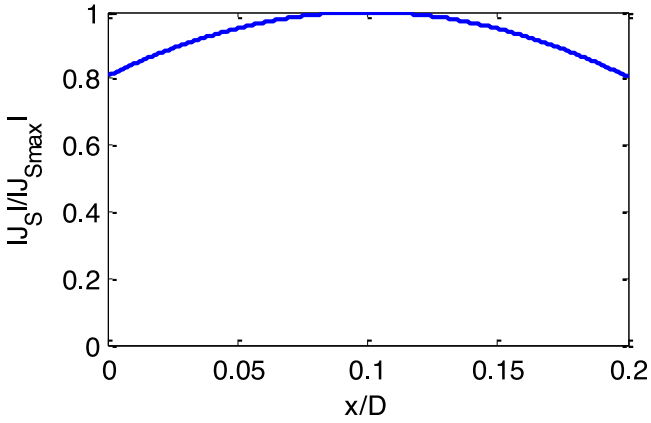

Fig. 5. The surface current density on graphene at resonant wavelength.

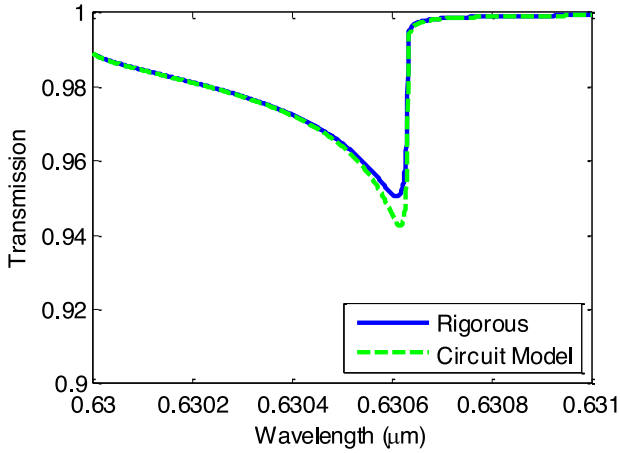

Fig. 6. Transmission of the structure shown in Fig. 1 at normal incidence and with $D = 630$ nm, $W = 0.2\ D$, $n_1 = 1$ and $n_2 = 1.001$. A five-layer graphene is used in this simulation. The resonance disappears due to the slight difference of the refractive indexes.

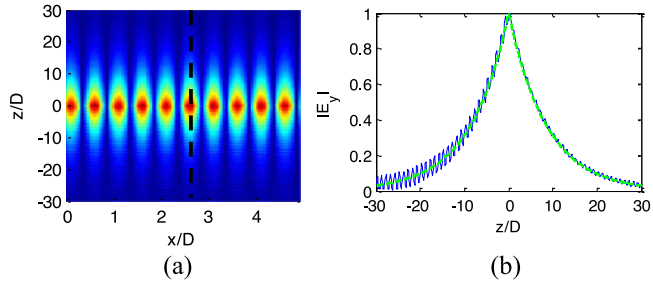

Fig. 7. (a) The magnitude of electric field ($|E_y|$) at resonance. (b) The distribution of $|E_y|$ along the dashed line on the left figure (blue solid line) and the electric distribution of a TE guided mode whose propagation constant is calculated using (6) (green dashed line). The parameters of the structure are the same as Fig. 4.

function. This sinusoidal profile is due to the excitation of a guided mode which will be discussed later in this section.

A slight mismatch between the refractive indexes of the upper and the lower mediums leads to disappearance of the resonance. It is demonstrated in Fig. 6 where the refractive index of the lower medium is changed to $n_2 = 1.001$.

Now let us consider this structure from another point of view: graphene can be regarded as an ultrathin dielectric with a refractive index of $n_G = \sqrt{1 - j\sigma_s/(\omega\varepsilon_0\Delta)}$ where $\Delta = 0.34$ nm is the approximate thickness of graphene [20]. Therefore, the graphene layer studied in the previous examples can be considered as an ultrathin dielectric layer whose refractive index is $n_G = 2.68 - 0.0094j$ at $\lambda = 630$ nm. (For *k* layers of graphene the thickness is $\Delta = 0.34k$ nm, however the refractive index is unchanged because, as mentioned before, the surface conductivity is also multiplied by *k*). Therefore, the PAGR may be considered as an ultra-thin dielectric grating which is known to support a TE guided mode. Under the TE incidence this mode is excited and a guided mode resonance is observed. Although the in-plane momentum of the incident light is zero (normal incidence), the momentum of the first diffracted order can be matched to that of the TE guided mode. Therefore, the propagation constant of the mode can be obtained by writing the momentum matching condition:

$$\beta_{\mathrm{TE}} = \frac{2\pi}{D}. \tag{6}$$

The electric field profile of the previous example at the resonance wavelength of $\lambda = 630.109$ nm is shown in Fig. 7(a), which clearly demonstrates the excitation of a guided mode. Inasmuch as the excitation is normal, the right- and left propagating modes are both excited and as a result the field distribution has a standing wave characteristic with two maxima in one period. This is also the reason that we observed a sinusoidal profile in Fig. 5. In Fig. 7(b), the electric field along the dashed line in Fig. 7(a), is shown (blue solid line) and, for the sake of comparison, the electric field distribution of a TE guided mode whose propagation constant is given by (6) as $\beta_{\mathrm{TE}} = 1.00017(2\pi/\lambda)$, is also plotted (green dashed line). The excellent agreement demonstrates the excitation of the TE guided mode.

The above argument shows that the well-known resonant reflection from a pure dielectric grating [21] in the case of thin dielectric ribbons can be well explained by the proposed circuit model. As a numerical example consider an array of dielectric ribbons with refractive index of $n_R = 2$ and thickness

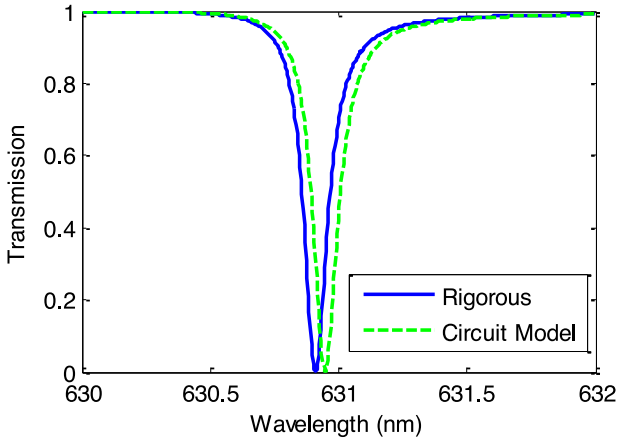

Fig. 8. Transmission of a TE polarized plane wave from a periodic array of dielectric ribbons. The refractive index of ribbons is $n_R = 2$ and their thickness is $\Delta = 10$ nm.

of $\Delta = 10$ nm in free space, illuminated by a TE plane wave at normal incidence. The period of the array and the width of ribbons are the same as the pervious examples. Transmission of the structure is plotted in Fig. 8 and a sharp resonance is observed at $\lambda = 630.91$ nm with bandwidth of $\Delta\lambda$ 0.1 nm. The rigorous results are obtained by using FMM with adaptive spatial resolution [22], and for circuit model the dielectric ribbons are considered as zero-thickness surface conductivities with $\sigma_s = j\omega\varepsilon_0\Delta\left(n_R^2 - 1\right)$.

An interesting feature of the studied resonance is its extraordinary sharpness, especially in the case of the graphene array. Improvement of quality factor $(Q = \lambda/\Delta\lambda)$ with the decrease of thickness can be easily explained by the circuit model. For a series *LC* resonance the quality factor is inversely proportional to the capacitance. On the other hand, from (5), it is obvious that the capacitance is decreased by the reduction of surface conductivity. So the maximum quality factor is achieved for the minimum surface conductivity which is, in turn, proportional to the dielectric thickness for a fixed refractive index.

Let us examine the behavior of the quality factor quantitatively. Consider again the second numerical example: the PAGR made of a five-layer graphene, the quality factor as a function of ribbons width is plotted in Fig. 10(a). The quality factor depends on two parameters: the intrinsic loss due to material absorption and the coupling to external waves. So the total quality factor reads as [23],

$$\frac{1}{Q_{tot}} = \frac{1}{Q_{sca}} + \frac{1}{Q_{abs}} \tag{7}$$

where Q_{sca} and Q_{abs} are the quality factors of scattering and absorption processes, respectively. Q_{sca} can be easily obtained by simulating the structure without material absorption, i.e., by setting $\tau^{-1} = 0$ in (1). After calculating Q_{tot} and Q_{sca} by means of numerical simulation, Q_{abs} can be easily calculated by (7).

The intrinsic loss is proportional to the graphene width and thus, Q_{abs} is a decreasing function versus *W/D*, as shown in Fig. 9(a). On the other hand, the loss due to the coupling increases when the waveguide is more perturbed, so the minimum

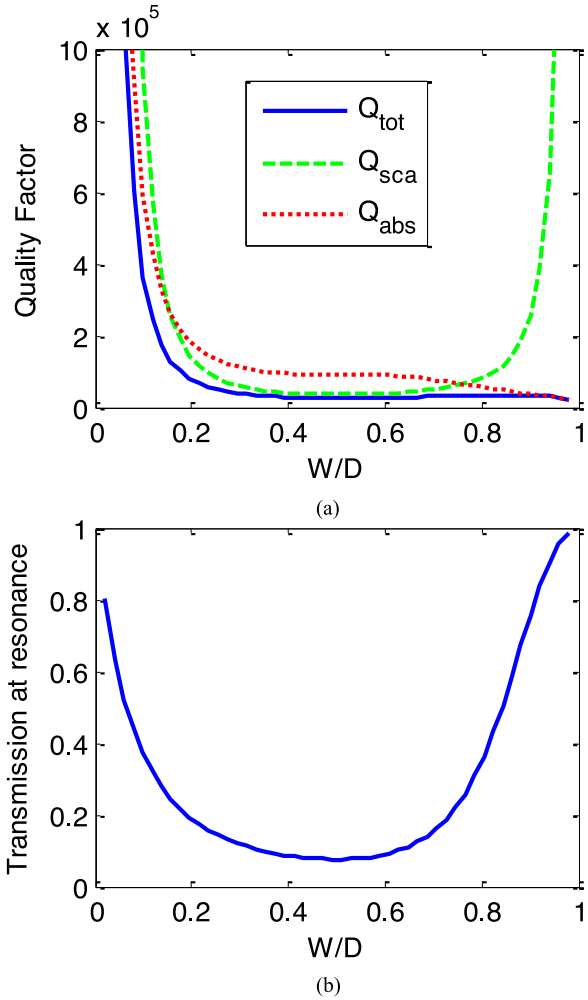

Fig. 9. (a) The quality factor and (b) transmission at resonance in terms of *W/D*. The quality factors due to scattering and intrinsic material loss are also plotted.

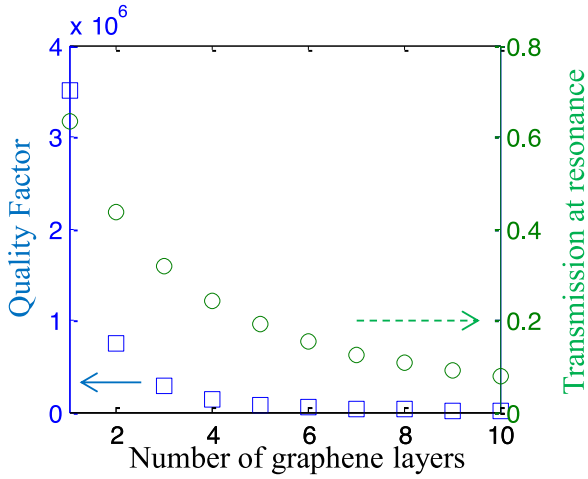

Fig. 10. The quality factor (squares) and transmission at resonance (circles) of the PAGR in terms of number of graphene layers.

of Q_{sca} is observed at $W/D = 0.5$. The behavior of Q_{tot} is more complex and it is determined by (7).

The transmission of the structure at resonance versus *W/D* is also plotted in Fig. 9(b). The minimum transmission is seen around $W/D = 0.5$. Therefore, the resonance is deeper, and thus more detectable, in this situation. On the other hand, when $W/D \to 0$ and $W/D \to 1$, the transmission at resonance tends to unity, which means that the transmission resonance disappears.

The quality factor and transmission at resonance, in terms of the number of graphene layers, are also illustrated in Fig. 10. It is seen that the quality factor is rapidly decreasing as a function of the number of graphene layers. It is also obvious that the transmission at resonance is a decreasing function. It should be noted that if the graphene was lossless, the transmission at resonance would be zero.

To design a desired structure, the quality factor can be tuned by means of the number of graphene layers. For sensing applications higher quality factor is preferred, but resonances with too high quality factors may not be detectable and thus appropriate quality factor depends on the frequency resolution of the detector. The transmission at resonance, on the other hand, can be well adjusted by the width to period ratio and the deepest resonance is achieved for $W/D = 0.5$.

IV. Conclusion

In summary, a circuit model was proposed for PAGRs in TE polarization. It was shown that PAGRs possess dual capacitive-inductive nature at high frequencies ($\hbar\omega > 1.667\, E_F$), and this can lead to an ultra-sharp *LC* resonance. The resonance predicted by the circuit model was also observed in full-wave simulations. The resonance was too narrowband in the case of monolayer graphene. However, it was demonstrated that the bandwidth can be increased by using multiple graphene layers. Moreover, it was shown that since the graphene layer can be considered as an ultrathin dielectric layer, the observed phenomenon is indeed the well known resonant reflection from a dielectric array in the extreme limit of one-atom thickness.

The quality factor of the resonance and its transmission ratio in terms of width to period ratio of ribbons and number of graphene layers were studied, and the effect of these parameters on the resonance was discussed.

The effect studied in this work, may be important for sensing applications [24], and all-optical bistable switching [25].

Acknowledgment

The author would like to thank Dr. B. Rejaei for revising this paper and many enlightening discussions.

References

[1] K. S. Novoselov, A. K. Geim, S. V. Morozov, D. Jiang, Y. Zhang, S. V. Dubonos, I. V. Grigorieva, and A. A. Firsov, "Electric field effect in atomically thin carbon films," *Science*, vol. 306, no. 5696, pp. 666–669, 2004.

[2] A. K. Geim and K. S. Novoselov, "The rise of graphene," *Nature Mater.*, vol. 6, no. 3, pp. 183–191, 2007.

[3] A. N. Grigorenko, M. Polini, and K. S. Novoselov, "Graphene plasmonics," *Nature Photonics*, vol. 6, no. 11, pp. 749–758, 2012.

[4] Y.-M. Lin, K. A. Jenkins, A. Valdes-Garcia, J. P. Small, D. B. Farmer, and P. Avouris, "Operation of graphene transistors at gigahertz frequencies," *Nano Lett.*, vol. 9, no. 1, pp. 422–426, 2008.

[5] M. Liu, X. Yin, E. Ulin-Avila, B. Geng, T. Zentgraf, L. Ju, F. Wang, and X. Zhang, "A graphene-based broadband optical modulator," *Nature*, vol. 474, no. 7349, pp. 64–67, 2011.

[6] F. Xia, T. Mueller, Y. Lin, A. Valdes-Garcia, and P. Avouris, "Ultrafast graphene photodetector," *Nature Nanotechnol.*, vol. 4, no. 12, pp. 839–843, 2009.

[7] S. Bae, H. Kim, Y. Lee, X. Xu, J.-S. Park, Y. Zheng, J. Balakrishnan, T. Lei, H. R. Kim, and Y. I. Song, "Roll-to-roll production of 30-inch graphene films for transparent electrodes," *Nature Nanotechnol.*, vol. 5, no. 8, pp. 574–578, 2010.

[8] L. Ju, B. Geng, J. Horng, C. Girit, M. Martin, Z. Hao, H. A. Bechtel, X. Liang, A. Zettl, and Y. R. Shen, "Graphene plasmonics for tunable terahertz metamaterials," *Nature Nanotechnol.*, vol. 6, no. 10, pp. 630–634, 2011.

[9] S. Thongrattanasiri, F. H. Koppens, and F. J. García de Abajo, "Complete optical absorption in periodically patterned graphene," *Phys. Rev. Lett.*, vol. 108, no. 4, p. 047401, 2012.

[10] A. Y. Nikitin, F. Guinea, F. J. Garcia-Vidal, and L. Martin-Moreno, "Surface plasmon enhanced absorption and suppressed transmission in periodic arrays of graphene ribbons," *Phys. Rev. B*, vol. 85, no. 8, p. 081405, 2012.

[11] M. Amin, M. Farhat, and H. Bağcı, "An ultra-broadband multilayered graphene absorber," *Opt. Exp.*, vol. 21, no. 24, pp. 29938–29948, 2013.

[12] Y. R. Padooru, A. B. Yakovlev, P.-Y. Chen, and A. Alù, "Analytical modeling of conformal mantle cloaks for cylindrical objects using subwavelength printed and slotted arrays," *J. Appl. Phys.*, vol. 112, no. 3, p. 034907, 2012.

[13] Y. R. Padooru, A. B. Yakovlev, C. S. Kaipa, G. W. Hanson, F. Medina, and F. Mesa, "Dual capacitive-inductive nature of periodic graphene patches: Transmission characteristics at low-terahertz frequencies," *Phys. Rev. B*, vol. 87, no. 11, p. 115401, 2013.

[14] A. Khavasi and B. Rejaei, "Analytical modeling of graphene ribbons as optical circuit elements," *IEEE J. Quantum Electron.*, vol. 50, no. 6, pp. 397–403, Jun. 2014.

[15] V. W. Brar, M. S. Jang, M. Sherrott, J. J. Lopez, and H. A. Atwater, "Highly confined tunable mid-infrared plasmonics in graphene nanoresonators," *Nano Lett.*, vol. 13, no. 6, pp. 2541–2547, 2013.

[16] G. Kafaie, A. Khavasi, and K. Mehrany, "Accurate effective medium theory for arrays of metallic nanowires," *J. Opt.*, vol. 17, no. 2, p. 025104, 2015.

[17] G. W. Hanson, "Dyadic Green's functions and guided surface waves for a surface conductivity model of graphene," *J. Appl. Phys.*, vol. 103, no. 6, p. 064302, 2008.

[18] A. Khavasi and K. Mehrany, "Circuit model for lamellar metallic gratings in the sub-wavelength regime," *IEEE J. Quantum Electron.*, vol. 47, no. 10, pp. 1330–1335, Oct. 2011.

[19] S. Mikhailov and K. Ziegler, "New electromagnetic mode in graphene," *Phys. Rev. Lett.*, vol. 99, no. 1, p. 016803, 2007.

[20] A. Khavasi, "Fast convergent Fourier modal method for the analysis of periodic arrays of graphene ribbons," *Opt. Lett.*, vol. 38, no. 16, pp. 3009–3012, 2013.

[21] G. Golubenko, A. Svakhin, V. A. Sychugov, and A. V. Tishchenko, "Total reflection of light from a corrugated surface of a dielectric waveguide," *Quantum Electron.*, vol. 15, no. 7, pp. 886–887, 1985.

[22] A. Khavasi and K. Mehrany, "Adaptive spatial resolution in fast, efficient, and stable analysis of metallic lamellar gratings at microwave frequencies," *IEEE Trans. Antennas Propag.*, vol. 57, no. 4, pp. 1115–1121, Apr. 2009.

[23] G. Palasantzas, "Quality factor due to roughness scattering of shear horizontal surface acoustic waves in nanoresonators," *J. Appl. Phys.*, vol. 104, no. 5, p. 053524, 2008.

[24] L. Meng, D. Zhao, Z. Ruan, Q. Li, Y. Yang, and M. Qiu, "Optimized grating as an ultra-narrow band absorber or plasmonic sensor," *Opt. Lett.*, vol. 39, no. 5, pp. 1137–1140, 2014.

[25] M. F. Yanik, S. Fan, and M. Soljačić, "High-contrast all-optical bistable switching in photonic crystal microcavities," *Appl. Phys. Lett.*, vol. 83, no. 14, pp. 2739–2741, 2003.

Amin Khavasi was born in Zanjan, Iran, on January 22, 1984. He received the B.Sc., M.Sc., and Ph.D. degrees from the Sharif University of Technology, Tehran, Iran, in 2006, 2008, and 2012, respectively, all in electrical engineering.

Since 2012, he has been at the Department of Electrical Engineering, Sharif University of Technology, where he is currently an Assistant Professor. His research interests include plasmonics, periodic structures, and circuit modeling of photonic structures.